Hindawi
Journal of Nanomaterials
Volume 2021, Article ID 6668393, 11 pages
https://doi.org/10.1155/2021/6668393

Research Article

Fabrication of Hierarchical Nanocomposites through a Nature-Mimic Method: Depositing MoS_2 Nanoparticles on Carbon Nitride Nanotubes by Polydopamine Coating

Yansong Wu,[1] Wei Ding,[1] and Jian Li[1,2]

[1]*College of Chemistry and Chemical Engineering, Northeast Petroleum University, Heilongjiang, Daqing 163318, China*
[2]*School of Material Science and Chemical Engineering, Tianjin University of Science and Technology, Tianjin 300457, China*

Correspondence should be addressed to Jian Li; lijian@tust.edu.cn

Received 27 November 2020; Revised 2 April 2021; Accepted 28 April 2021; Published 20 May 2021

Academic Editor: Marinella Striccoli

The combination of 1D nanotubes with 0D nanoparticles to integrate a nanocomposite structure has attracted increasing research interest, while the interfacial interaction plays an important role in such composites. This paper presents a facile and universal approach for the fabrication of hierarchical NP-NT nanocomposites with improved photocatalytic performances by mussel chemistry. Polydopamine (PDA) serves as the biomimetic adhesive layer and then connects MoS_2 nanoparticles with g-C_3N_4 nanotubes (CNNTs). The obtained nanocomposites were characterized by FT-IR spectra, XRD, SEM, TEM, XPS, UV-vis DRS, and PL. Compared with unmodified CNNTs, the *as*-prepared MoS_2-PDA-CNNT composites exhibited an enhanced photocatalytic properties for the degradation of methylene blue (MB) under visible light irradiation. This research would provide a green and versatile method to construct hierarchical structured nanocomposites with high catalytic activity.

1. Introduction

For the past few years, graphic carbon nitride (g-C_3N_4) attracts increasing interest in the research areas of photocatalytic water splitting [1, 2], organic synthesis [3], and degradation of pollutants [4–7]. Generally, the g-C_3N_4 has been widely utilized in many research areas due to its steady physical-chemical properties, narrow band gap, and inexpensive preparation cost [8]. However, the drawbacks of g-C_3N_4 such as its bulk layered structure, rapid photogenerated recombination of electron–hole (e^-–h^+) pair, and low efficiency in the use of visible light induce a low visible-light activity, which limited its further applications [9]. The nanostructural design of g-C_3N_4 and the development of heterostructured nanocomposites based on g-C_3N_4 are two main methods for improving the photocatalytic performance of g-C_3N_4 under visible light irradiation. By the first method, metals [10], metal oxides [11], metal sulfides [12], and some other components [13] were usually used to modified g-C_3N_4. Besides, g-C_3N_4 with hierarchical nanostructures such as mesopores [9], nanorods [14],, nanosheets [15] (hollow), nanospheres [16, 17], and nanotubes [18, 19] was also successfully constructed by the researchers. As one known, a tubular nanostructure can provide both internal and external exposed active sites for photocatalytic reactions, promote photogenerated electron transfer, and reduce the resistance to mass transfer of photocatalytic reactions. Huang and coauthors [20] fabricated porous g-C_3N_4 nanotubes by heating precursors synthesized by melamine recrystallization from H_2SO_4/methanol mixed solution. Compared with bulk g-C_3N_4 obtained by direct pyrolysis, the porous g-C_3N_4 nanotubes exhibit improved photocatalytic activity for the photocatalytic water splitting into hydrogen under visible light irradiation.

Over the past decade, integrating 1D nanotubes with 0D nanoparticles (NP) to develop a hybrid structure has aroused great interest. This hybridization often leads to intriguing structural, electromagnetic, electrochemical, and photochemical properties which were not shown by the separate components alone [21, 22]. For instance, Li's group [21] deposited carbon nitride nanotubes with platinum nanoparticles (Pt/CNNT) by a facile one-pot solvothermal treatment

method. Pt/CNNTs as prepared exhibited improved visible light photocatalytic activity toward the water splitting as well as pollutant degradation [21].

Nevertheless, it is still so challenging to strongly bind the NPs onto NTs due to the weak binding interaction between them [23]. Traditionally, researchers have introduced oxygen-containing functional groups (such as -OH, -COOH, or -C=O) through a complex process of surface modification to strongly anchor the NPs on the NTs.

In nature, 3,4-dihydroxy-L-phenylalanine (dopamine, DA) was abundant in marine mussel adhesive proteins (MAPs). Interestingly, it is via the oxidation of the catechol group in a slightly alkaline solutions (pH > 7.5), and DA can easily self-polymerize and be coated on many types of organic or inorganic substrates [24]. Yu et al. [25] employed polydopamine (PDA) to modify the surface of bulk graphic carbon nitride, and the PDA-g-C_3N_4 exhibited increasing photocatalytic activity. Due to its versatile adhesion ability, PDA is utilized as the connecting layer to decorate substrates with NPs. In addition, polydopamine can provide an efficient platform for complementary interface reactions. In particular, functional groups such as the amine (–NH_2) and catechol/quinine group (–OH/=O) at the ring can serve as good ligands for binding metal ion and reducing noble metal ions to noble metal NPs [25].

Recently, molybdenum sulfide- (MoS_2-) based catalysts have attracted interest in the field of photocatalysis. It was utilized in photocatalytic water splitting into hydrogen [26] as well as in the degradation of various dyes [27], due to its narrow band gap [28] (visible to near-infrared), high absorption of visible light, low toxicity, and abundant of active sites. Meanwhile, because of its too narrow band gap and low quantum efficiency, MoS_2 has been widely used as a cocatalyst for creating heterostructure with Bi_2O_3 [29], MoO_3 [30], ZnO [31], and especially g-C_3N_4 [26, 32].

Inspired by the aforementioned researches, we modified carbon nitride nanotubes (PDA-CNNTs) by polydopamine coating. Due to this biomimetic adhensive PDA layer, MoS_2 nanoparticles were easily deposited. Specifically, the structure, morphology, and photocatalysis properties of the *as*-prepared MoS_2-PDA-CNNT nanocomposites have been systematically studied.

2. Materials and Methods

2.1. Materials. Melamine and MoS_2 nanoparticles were purchased from Jiang Tian Chemical Technology Co. Ltd. (Tianjin China). 3,4-Dihydroxyphenethylamine hydrochloride (DA, 98%) was purchased from Shanghai Aladdin Biochemical Technology Co. Ltd. (Shanghai China). All the other chemicals were purchased locally. All chemicals are analytical reagent (AR) grade.

2.2. Preparation

2.2.1. Preparation of g-C_3N_4 Nanotubes. The preparation of the holey g-C_3N_4 nanotubes (CNNTs) is according to the published literature with some modification [33]. Typically, melamine (520 mg) was added in ethylene glycol (20 mL) and stirred for dissolution under room temperature. The 0.12 mol L^{-1} nitric acid aqueous solution (60 mL) was added dropwise to the above solution. The reaction is stopped after stirring for 10 min. After collecting the generated precipitation by centrifugation and washing three times using ethanol, vacuum drying at 55°C for 8 h was applied to remove the volatile solvent. The obtained white precursor was annealed at 350°C for 1 h using a heating rate of 8°C·min^{-1}. The *as*-prepared samples are denoted as CNNTs.

2.2.2. Preparation of Dopamine/g-C_3N_4 Nanotubes. PDA-CNNTs were fabricated by a solution method. In brief, of dopamine-hydrochloride added to the aqueous dispersion of CNNTs for 24 h, CNNTs (500 mg) were dispersed into 100 mL deionized H_2O, and the suspension was under continuously ultrasonic treatment. After about 30 min, a certain amount of dopamine-hydrochloride was added to the above suspension. And then the mixture suspension was for 60 min under continuously stirring at room temperature. A desired concentration of Tris-HCl solution (100 mL) was added, and 1 mol L^{-1} NaOH solution was added to adjust the pH (pH = 8.5) of the mixture. The polydopamine coated g-C_3N_4 nanotubes (PDA-CNNTs) were obtained by centrifugation [25].

2.2.3. Preparation of MoS_2/Dopamine/g-C_3N_4 Nanotubes. PDA-CNNTs were redispersed in 10 mmol L^{-1} Tris buffer solution (500 mL, pH 8.5), and then 500 mg nano-MoS_2 nanoparticles were added to the solution with magnetically stirred vigorously at 60°C for 24 h. And then the unreacted dopamine and MoS_2 nanoparticles were removed by Tris-HCl buffer and deionized water three times, and solid samples were collected by centrifugation. Finally, the composite was dried at 60°C in air for 24 h and is denoted as MoS_2-PDA-CNNTs.

2.3. Characterization. The scanning electron microscopy (SEM, Philips XL30 ESEM, and Hitachi S-4800 instrument at an operation voltage of 20.0 keV and 0.7 keV) and transmission electron microscopy (TEM; Tecnai G2 F20 with accelerating voltage of 200 kV) were performed to observe the surface morphology and microstructures of *as*-prepared samples. Fourier transform infrared spectra (FTIR) of the samples were measured on FTIR Spectrometer (FTIR; Bruker Tensor 27). The power X-ray diffraction (XRD) was tested by an XRD-6100X diffractometer (Shimadzu, Japan) with a Cu Kα source. The scan rate is 2° min^{-1} (from 5° to 70°). The X-ray photoelectron spectroscopy (XPS) was tested by XPS spectroscopy (Thermo Fisher Scientific, UK). The UV-vis diffuse reflectance spectra (UV-vis DRS) were measured on a UV-3600 Plus spectrometer (Shimadzu, Japan). The photoluminescence measurements (PL) were recorded on fluorescence spectrophotometer (F-7000, Hitachi, Japan) with 273 nm laser illumination.

2.4. Photocatalytic Experiments. The photocatalytic degradation efficiency of pure CNNTs and composites was evaluated by removal of methylene blue (MB) under visible light irradiation [25]. The visible light source was a 500 W Xe lamp (λ > 420 nm), and the illumination distance was kept at about

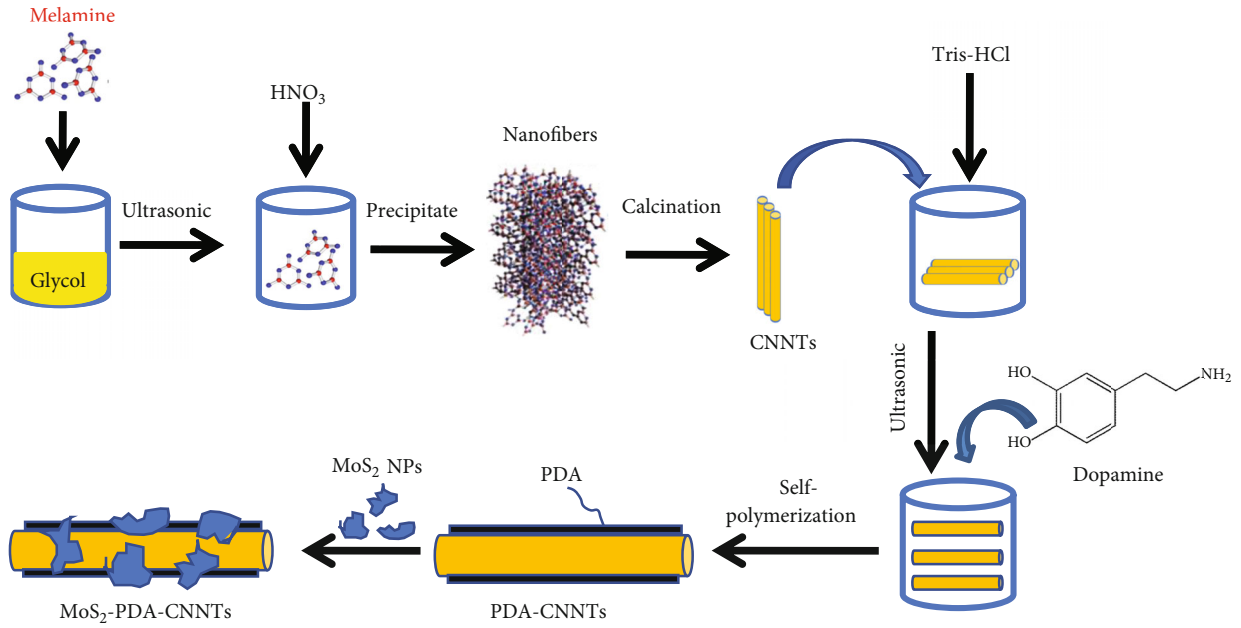

Scheme 1: Illustrations for the preparation of the MoS_2-PDA-CNNTs composites.

15 cm. The reaction temperature is about 25°C. Typically, the *as*-prepared photocatalyst (100 mg) was dispersed in 20 mg·L^{-1} MB solution (100 mL). Prior to light irradiation, the system was under magnetically stirring in the dark for 30 min to ensure the *as*-prepared photocatalyst reach the adsorption equilibrium. After certain time intervals (30 min), the reaction solution was collected by centrifugation to remove the *as*-prepared photocatalyst for subsequent analysis. The residual concentrations of MB were monitored by UV-vis spectroscopy (UV-762; Shanghai China), and the photodegradation efficiency was calculated.

3. Results and Discussion

The tentative formation mechanism of MoS_2-PDA-CNNTs was schematically illustrated in Scheme 1. The process included four steps: melamine dissolving, self-assembly to 1D fibrous, thermalized to tubular structure, biomimetic coating, and nanoparticle depositing. Melamine could be slightly dissolved in ethylene glycol, and then dropwise addition of an aqueous solution of nitric acid to the glycol solution saturated with melamine gradually leads to a white precipitation consists of a fibrous structure. In the above process, we can easily protonate the melamine by reacting the amine in melamine with HNO_3, thereby reducing its solubility in ethylene glycol. The protonated melamine self-assembled with nitrate ions and turned into fibrous structures. With a heating process, the protonated melamine forms tris-s-triazine rings and polymerizes to form molecular ribbons. Then, the molecular ribbons overlap each other and form stable stacking layers of a certain thickness through p-p electron interaction. Next, the stacking layer tends to roll up into nanotubes due to the driving force for minimizing surface free energy. The fibrous structures transformed to nanotubular [33]. Next, the freshly prepared CNNTs were subject to partially crosslinking reaction with DA in a Tris buffer of pH = 8.5. The partial crosslinking process caused by a Schiff base/Michael addition reaction, that is, the interaction between the catechol group of DA/PDA and the primary amine group of CNNTs. After applying the PDA layer onto the CNNTs, MoS_2 nanoparticles were coated onto the surface inspired by dopamine chemistry, and the MoS_2-PDA-CNNTs were obtained.

The morphology and microstructure of the obtained pure CNNTs and the composites were investigated using scanning electron microscopy (SEM) and transmission electron microscopy (TEM). As can be seen from Figures 1(a) and 1(b), the outer diameter of *as*-prepared CNNTs is ranging from 300 to 500 nm, and the length of CNNTs reaches several millimeters. The corresponding TEM image (Figure 1(e)) further confirmed the morphology of the tubular elements with pore penetration across the tube wall (as arrows marked in Figure 1(b)) [33]. The TEM image reveals that the thickness of CNNTs wall was measured to approximately 30 nm. The unique properties of these CNNTs will make them very suitable for photocatalytic reaction. Moreover, there are enough published references to prove that the thin tubular structure can promote photocharge separation and inhibit the charge recombination. At the meantime, the tubular structure and the pores into the tube wall should promote the mass transfer of reactants and products, which will also facilitate the photocatalytic reactions. After modifying PDA and subsequent MoS_2 on the surface of CNNTs, the overall tubular morphology of CNNTs was still preserved, as shown in the SEM (Figure 1(d)) and TEM images (Figure 1(e)). The corresponding TEM image also indicates that some MoS_2 protruded nanoparticles have been successfully grafted onto the surface of PDA-CNNTs. The energy-dispersive X-ray spectroscopy (EDS) indicated that only the elements C to O mass ratio were increased while the N was

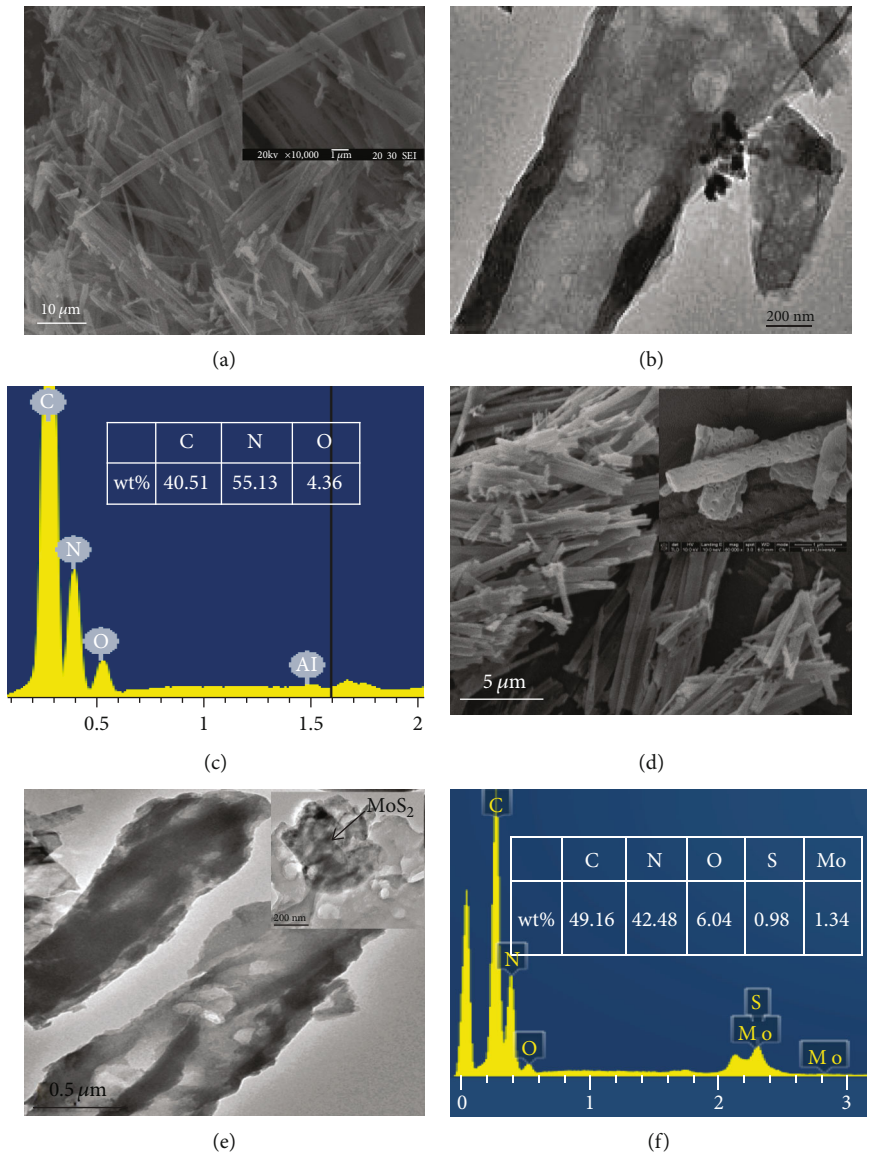

Figure 1: (a) SEM, (b) TEM, and (c) EDS of CNNTs. (d) SEM of PDA-CNNTs. (e) TEM and (f) EDS of MoS_2-PDA-CNNT nanocomposites.

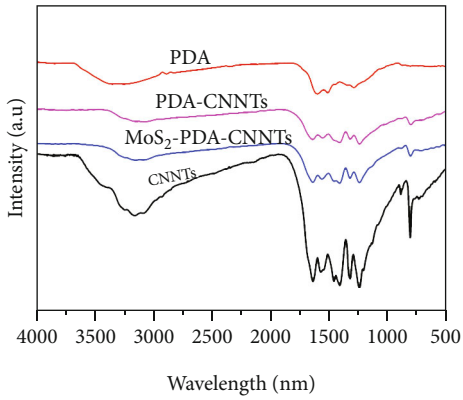

Figure 2: FTIR spectra of CNNTs and nanocomposites.

decreased due to the PDA coating. In addition, Mo and S element was indeed distributed in the MoS_2-PDA-CNNTs [34].

Figure 2 shows FTIR spectra of CNNTs and composites. The characteristic peaks ranging from 1200 to 1650 cm^{-1} were observed in the FTIR spectrum of CNNTs, corresponding to the typical stretching vibration signals of the g-C_3N_4 molecular structure [35]. The broad peaks at about 3051 and 1244 cm^{-1} were assigned to the stretching vibration of the C-NH-C linking groups due to partial polycondensation during the g-C_3N_4 formation [36]. In addition, the strong peaks at about 812 cm^{-1} are assigned to the breathing mode of the tri-s-triazine ring of g-C_3N_4 [35]. After the PDA and MoS_2 modification, the FTIR spectrum of PDA-CNNTs and MoS_2-PDA-CNNTs exhibited distinct peaks at about 3500-3055, 1594, 1224, and 1060 cm^{-1}, which were attributed to -OH/-NH, C=C, C-N, and C-O stretching vibrations, respectively. Meanwhile, the two peaks at 1534 and 1359 cm^{-1} were attributed to the C=N and C-N-C stretching

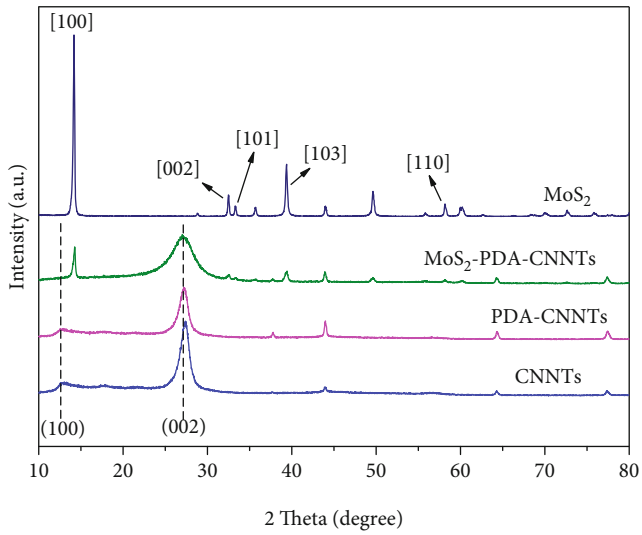

Figure 3: XRD spectra of CNNTs and composites.

vibration signals of indole ring in PDA. These clearly characteristic features indicated the successful self-polymerization of DA on the surface of CNNTs (Tris-HCl solution). Meanwhile, the FTIR spectra of PDA-CNNTs show strong peaks correspond to both g-C_3N_4 (tri-s-triazine ring) and PDA (stretching vibration of C-O). This result may be mainly due to the partial crosslinking process caused by a Schiff base/Michael addition reaction, that is, the interaction between the catechol (-OH) group of DA/PDA and the primary amine (-NH_2) group of CNNTs [37].

The X-ray diffraction (XRD) measurement was conducted to investigate the crystal structures of pure CNNTs, MoS_2, and composites, and the results were presented in the Figure 3. The XRD patterns of pure CNNTs show the presence of two mainly diffraction peaks at 13.35° and 27.69°, which were corresponded to the (100) and (002) planes, respectively. The strong diffraction peak at 27.69° of CNNTs was ascribed to the interlayer stacking reflection of conjugated aromatic systems, while the weak diffraction peaks at 13.35° represent the inplane trigonal nitrogen linkage of tri-s-triazine units. The calculated interlayer distance of CNNTs is 0.322 nm according to the XRD patterns [25]. According to PDF card no. 01-075-1539, the main diffraction peaks which were presented at 2theta 14.10°, 32.89°, 33.68°, 39.50°, and 58.73° matched well with the (002), (100), (101), (103), and (110) planes, respectively, attributable to MoS_2 [38], which were also showed in the spectra of MoS_2-PDA-CNNT composites.

Figure 4 shows XPS spectra of CNNTs and nanocomposites, which are used to investigate the surface chemical properties of the *as*-prepared samples. Compared to original CNNTs, we have observed new peaks belong to the S and Mo element in the MoS_2-PDA-CNNT composites, implying that the MoS_2 nanoparticles have been successfully decorated on the CNNTs surface. Figures 4(b)–4(f) show the high-resolution XPS spectra of Mo 3d, S 2p, C 1 s, N 1 s, and O 1 s. The C 1 s XPS spectra was deconvoluted into the three distinct peaks, C=C peak (at about 284.8 eV), C-N/C-OH peak (at about 286.3 eV), and C=N peak (at about 288.3 eV) (Figure 4(b)). Figure 4(c) shows that the N 1 s XPS spectra were deconvoluted into three peaks, which are C=N-C (at about 399.5 eV), N-(C)3 (at about 400.3 eV), and C-N-H (at about 401.4 eV). Figure 4(d) displays the O 1 s XPS spectra of MoS_2-PDA-CNNT composites. And the three peaks C=O (at about 531.9 eV), C-O (at about 532.8 eV), and adsorbed H_2O (at about 533.9 eV) indicate the presence of PDA [39]. Figure 4(e) shows two peaks at binding energies of about 232.5 and 229.3 eV correspond to the characteristic peaks of Mo $3d_{3/2}$ and Mo $3d_{5/2}$ of Mo^{4+} in MoS_2, respectively, while the two S 2p peaks at binding energies of 162 and 163.2 eV are attributed to the characteristic peaks of S^{2-} in MoS_2 [40]. All the above XPS results further confirmed the successful preparation of MoS_2-PDA-CNNT composites.

Figure 5(a) shows UV-vis diffuse reflectance absorption spectra of CNNTs and nanocomposites. All the *as*-prepared samples exhibited a high light absorption from 200 nm to 450 nm region. The inherent absorption edges of the samples originate from the charge transfer response from the valence band (VB) to the conduction band (CB). Compared to the bulk CNNTs, PDA-CNNTs and MoS_2-PDA-CNNTs exhibit the more pronounced light absorption abilities. The enhanced abilities may be due to the benefit of both the PDA layer and MoS_2 NPs for multiple reflections of the incident visible light. Figure 5(b) shows fluorescence spectra of CNNTs and nanocomposites with an excitation wavelength of 330 nm under room temperature. All the *as*-prepared samples show a wide range luminescence from 410 nm to 550 nm, and the peaks positions are centered at about 450 nm. This fluorescence phenomenon indicates that the photogenerated electrons and holes inevitably recombine in the semiconductors. It is worth noting that, compared with CNNTs and PDA-CNNTs, the PL intensity of MoS_2-PDA-CNNTs is significantly reduced, which suggested that the recombination degree of photogenerated carriers in the MoS_2-PDA-CNNTs sample is weakened [18].

The photocatalytic activity of the sample for degradation of MB is shown in Figure 6(a). When only light is provided without adding photocatalyst, almost no MB is degraded. The photodegradation activity of pure CNNTs is low, and only less than 60% of MB is photodegraded after 180 minutes. The sample MoS_2 nanoparticles showed the lowest photodegradation activity under 180 minutes of visible light irradiation. In previous research, PDA was proved to generate hydroxyl radicals under UV light irradiation [41]. To investigate its photo stability under visible light irradiation, the PDA particles as ref [41] were prepared and also catalyzed MB degradation. As shown in Figure S2, PDA presented high photo stability and negligible photocatalytic function. Measurements on MoS_2/CNNT samples show that the simply hydrothermal treating of the CNNTs with MoS_2 NPs had a tent of effect on the photocatalysis activity. The degradation rate of MB increased slightly for MoS_2/CNNTs. The PDA-modified CNNTs exhibited more obviously increase photocatalytic efficiency. Previous researches revealed the fact that PDA played a crucial role in the increasing photocatalytic activity and separating the electron-hole pairs [25]. Due to the synergic effect of the

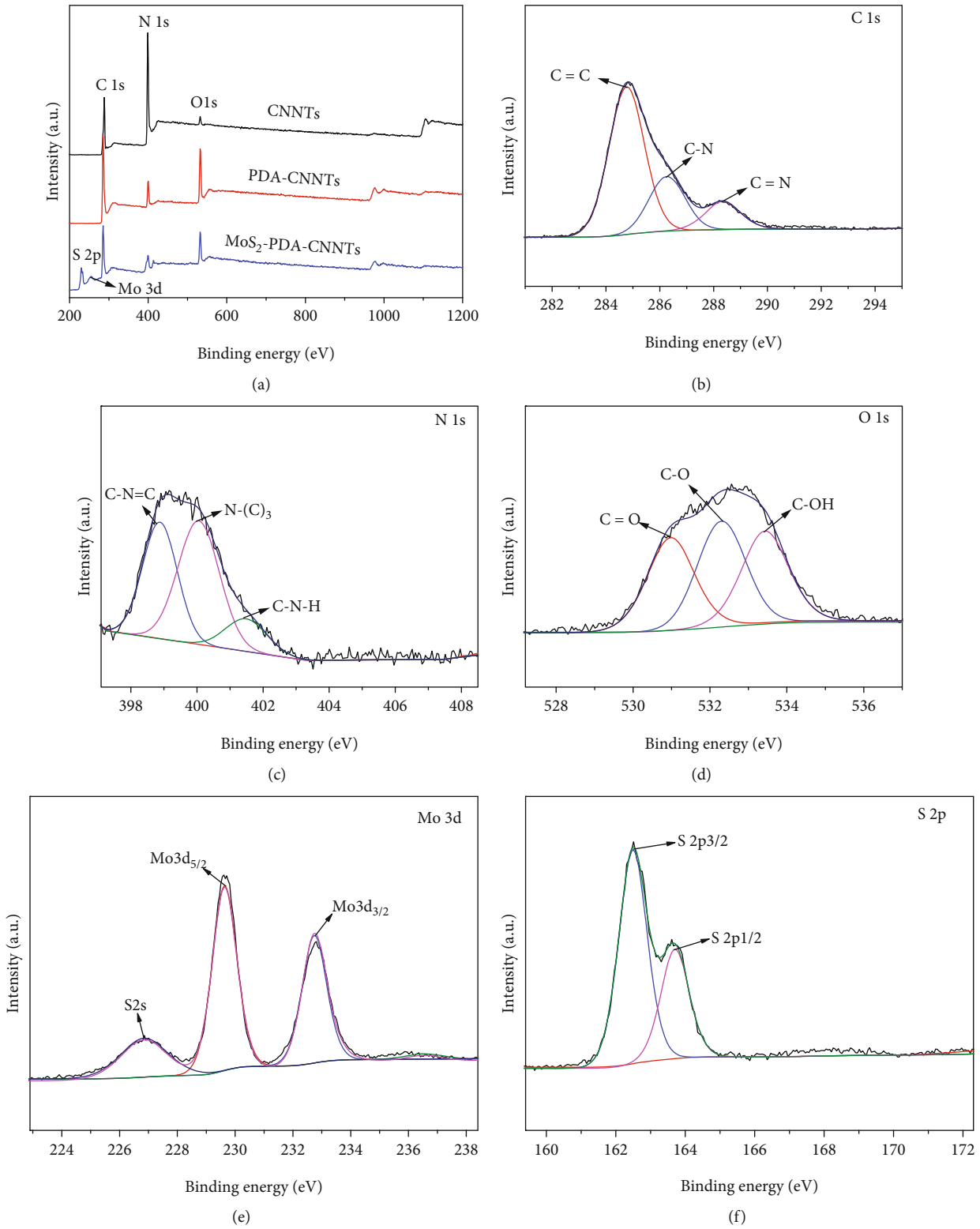

Figure 4: XPS survey spectra (a) and high-resolution of (b) C 1 s, (c) N 1 s, (d) O 1 s, (e) Mo 3d, and (f) S 2p spectra of CNNTs and nanocomposites.

PDA coating layer and MoS_2 nanoparticles, the photocatalytic activity of MoS_2-PDA-CNNT composite was the highest among the samples of Figure 6(a). The composite was also compared with previous reports, as listed in Table S1 [42–48]. The commercial benchmark TiO_2 P25 was also investigated under visible light irradiation. Its showed low photocatalytic activity for MB degradation. Since pure P25 cannot absorb visible light, its

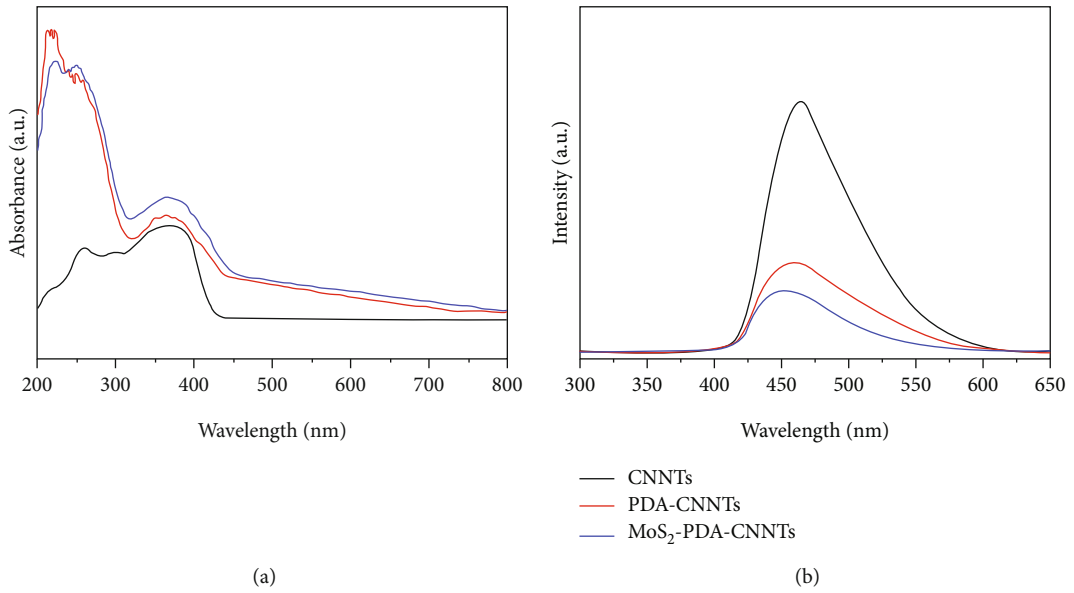

Figure 5: UV-vis diffuse reflectance absorption spectra (a) and fluorescence spectra (b) of CNNTs and nanocomposites.

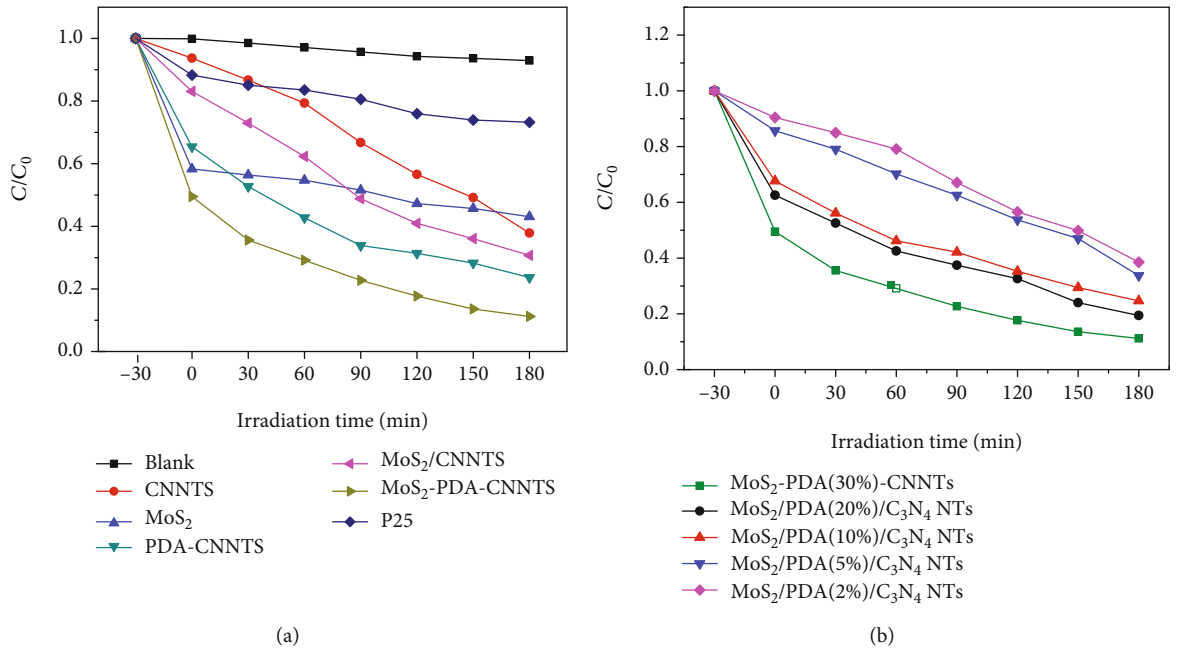

Figure 6: Photocatalytic degradation of MB under visible light.

slight MB photodegradation activity under visible light is due to the photosensitization of MB dye itself [42].

Besides, a colorless pollutant RhB was utilized in degradation to demonstrate the photocatalytic activity of MoS_2-PDA-CNNT composite (Figure S3). The results were similar with MB degradation, which also shown that the MoS_2-PDA-CNNTs have a well photocatalytic activity comparing with either pure g-C_3N_4 or MoS_2.

When the content of PDA was increased (Figure 6(b)), the photocatalytic activity of MoS_2-PDA-CNNT composites was enhanced that the degradation efficiency is gradually from 62% to 89%. The MoS_2-PDA- (30%-) CNNT sample presented the highest photocatalytic efficiency. This phenomenon is attributed to the fact that PDA can promote the light harvesting of the system through the electron and proton redox coupling method, thereby improving the photocatalytic activity. However, excessive PDA on the surface will produce a photogenerated electron shielding effect, which will hinder g-C_3N_4 from absorbing and utilizing the light source, reducing the photocatalytic activity of the system [25].

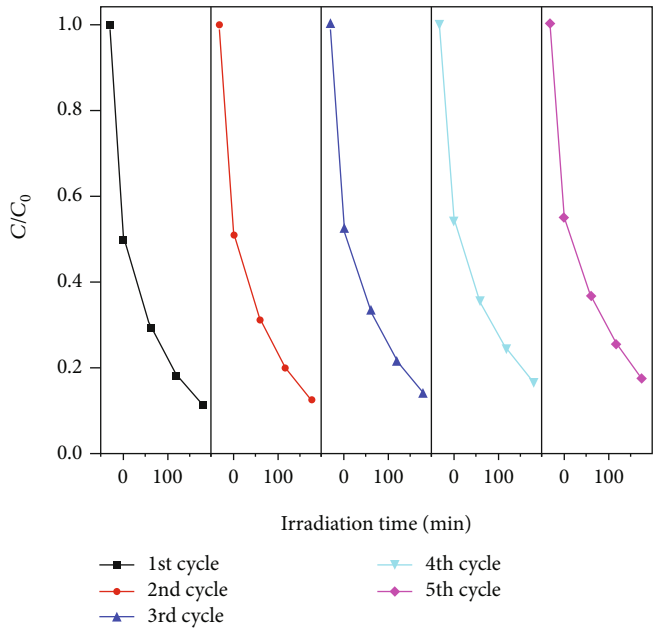

Figure 7: Recycling stability of MoS_2-PDA-CNNTs under visible light irradiation.

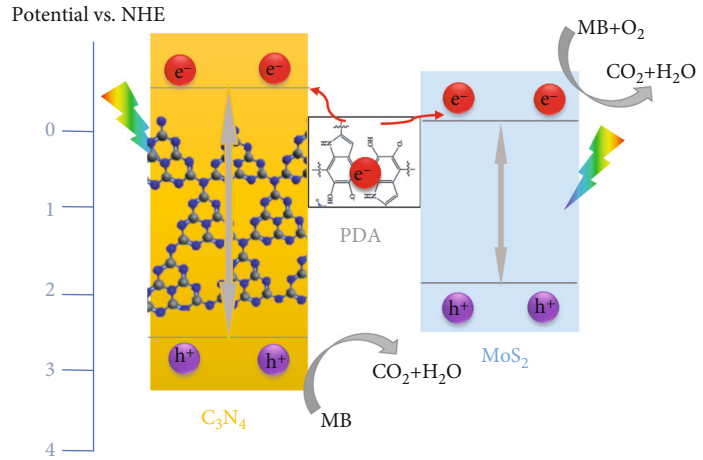

Figure 8: Schematic band structure diagram and the possible photocatalytic mechanism of MoS_2-PDA-CNNTs.

The reusing stability of MoS_2-PDA-CNNT composites was investigated via the cycle photodegradation of the MB under visible light irradiation ($\lambda > 400$ nm). After 5 cycles, only a little loss of degradation efficiency is observed, while the MoS_2-PDA-CNNTs still remain as photocatalytic activity as high as 89%, as shown in Figure 7. We also examined the stability of the used samples by the XRD patterns (Figure S4). It was found that the diffraction peak of the MoS_2-PDA-CNNT composites had no obvious discrepancy before and after five times of photocatalytic reaction. The results demonstrate that the photocatalyst owns good photocatalytic stability under visible light.

Figure 8 shows the schematic band structure diagram and the possible photocatalytic mechanism of MoS_2-PDA-CNNTs. Upon the irradiation with visible light, the electrons in the valence band edge (VB) of g-C_3N_4 and MoS_2 are excited and transferred to the conduction band edge (CB) and generating holes in the VB of g-C_3N_4 and MoS_2. The VB position values for g-C_3N_4 and MoS_2 are about -1.12 eV and -0.1 eV (vs. NHE), respectively [43]. The VB potential difference between g-C_3N_4 and MoS_2 facilitates the transfer of electrons from g-C_3N_4 to MoS_2. Besides, due to the interface modification of PDA with high electron transfer and separation ability, the electrons in the CB of g-C_3N_4 can quickly transfer to the CB of MoS_2. As a result, the recombination of photogenerated electrons and holes is hindered, and effective charge separation is achieved. The electrons in the CB of MoS_2 could react with O2 to form radicals (·OH or ·O2-). The radicals generated in the CB of MoS_2 and holes photogenerated in the VB of g-C_3N_4 are able to oxidize the MB to CO_2 and H_2O. The enhanced efficiency of photogenerated charge separation promotes the photocatalytic MB degradation activity of MoS_2-PDA-CNNTs.

4. Conclusions

In conclusion, a hierarchical NP-NT nanocomposite with enhanced photocatalytic properties was successfully constructed through a facile and versatile approach by mussel chemistry. Polydopamine (PDA) serves as the biomimetic adhesive layer which connects MoS_2 nanoparticles with g-C_3N_4 nanotubes (CNNTs). The MoS_2-PDA-CNNT composites presented improved visible light photocatalytic properties toward degradation of methylene blue (MB) due to the synergic effect of their unique tubular nanostructure, PDA coating layer, and MoS_2 nanoparticles. With the PDA ratio increasing, the photocatalyst light-harvesting performance was gradually enhanced. This research would provide a green, versatile strategy to fabricate hierarchical-structured nanocomposites with high catalytic activity.

Data Availability

All data used to support the findings of this study are available from the corresponding author upon request.

Conflicts of Interest

The authors declare no competing financial interests.

Acknowledgments

The authors thank the financial support from the Natural Science Foundation of Tianjin (18JCYBJC89200), the PetroChina Innovation Foundation (2018D-5007-0502, 2020D-5007-0405), and the Project from Tianjin Education Commission (2017KJ018, 2017KJ017).

Supplementary Materials

SEM images of MoS_2 nanoparticles (Figure S1), photocatalytic performances of PDA for MB degradation under visible light irradiation (Figure S2), photocatalytic degradation of RhB under visible light (Figure S3), XRD patterns of the MoS_2-PDA-C_3N_4 nanocomposites before and after recycling (Figure S4), and the reported catalysts for MB degradation (Table S1). *(Supplementary Materials)*

References

[1] S. Kumar, A. Kumar, V. Navakoteswara Rao, A. Kumar, M. V. Shankar, and V. Krishnan, "Defect-rich MoS2ultrathin nanosheets-coated nitrogen-doped ZnO nanorod heterostructures: an insight into in-situ-generated ZnS for enhanced photocatalytic hydrogen evolution," *ACS Applied Energy Materials*, vol. 2, no. 8, pp. 5622–5634, 2019.

[2] A. Bahuguna, A. Kumar, T. Chhabra, A. Kumar, and V. Krishnan, "Potassium-functionalized graphitic carbon nitride supported on reduced graphene oxide as a sustainable catalyst for Knoevenagel condensation," *ACS Applied Nano Materials*, vol. 1, no. 12, pp. 6711–6723, 2018.

[3] A. Kumar, P. Choudhary, K. Kumar, A. Kumar, and V. Krishnan, "Plasmon induced hot electron generation in two dimensional carbonaceous nanosheets decorated with au nanostars: enhanced photocatalytic activity under visible light," *Materials Chemistry Frontiers*, vol. 5, no. 3, pp. 1448–1467, 2021.

[4] L. Xiao, T. Liu, M. Zhang, Q. Li, and J. Yang, "Interfacial construction of Zero-Dimensional/One-Dimensional g-C3N4Nanoparticles/TiO2Nanotube arrays with Z-Scheme heterostructure for improved photoelectrochemical water splitting," *ACS Sustainable Chemistry & Engineering*, vol. 7, no. 2, pp. 2483–2491, 2019.

[5] T. Chhabra, A. Kumar, A. Bahuguna, and V. Krishnan, "Reduced graphene oxide supported MnO_2 nanorods as recyclable and efficient adsorptive photocatalysts for pollutants removal," *Vacuum*, vol. 160, pp. 333–346, 2019.

[6] J. Cai, J. Huang, S. Wang et al., "Crafting mussel-inspired metal nanoparticle-decorated ultrathin graphitic carbon nitride for the degradation of chemical pollutants and production of chemical resources," *Advanced Materials*, vol. 31, no. 15, article 1806314, 2019.

[7] A. Kumar, K. L. Reddy, S. Kumar, A. Kumar, V. Sharma, and V. Krishnan, "Rational design and development of lanthanide-doped NaYF4@CdS−au−RGO as quaternary plasmonic photocatalysts for harnessing visible−near-infrared broadband spectrum," *ACS Applied Materials & Interfaces*, vol. 10, no. 18, pp. 15565–15581, 2018.

[8] Y. Hou, Y. Zhu, Y. Xu, and X. Wang, "Photocatalytic hydrogen production over carbon nitride loaded with WS_2 as cocatalyst under visible light," *Applied Catalysis B: Environmental*, vol. 156-157, pp. 122–127, 2014.

[9] F. Goettmann, A. Fischer, M. Antonietti, and A. Thomas, "Chemical synthesis of mesoporous carbon nitrides using hard templates and their use as a metal-free catalyst for friedel-crafts reaction of benzene," *Angewandte Chemie International Edition*, vol. 45, no. 27, pp. 4467–4471, 2006.

[10] S. Le, T. Jiang, Q. Zhao et al., "Cu-doped mesoporous graphitic carbon nitride for enhanced visible-light driven photocatalysis," *RSC Advances*, vol. 6, no. 45, pp. 38811–38819, 2016.

[11] D. Chen, K. Wang, D. Xiang, R. Zong, W. Yao, and Y. Zhu, "Significantly enhancement of photocatalytic performances via core-shell structure of @mpg-C_3N_4," *Applied Catalysis B: Environmental*, vol. 147, pp. 554–561, 2014.

[12] Y. Zhong, J. Yuan, J. Wen et al., "Earth-abundant NiS cocatalyst modified metal-free mpg-C_3N_4/CNT nanocomposites for highly efficient visible-light photocatalytic H-2 evolution," *Dalton Transactions*, vol. 44, no. 41, pp. 18260–18269, 2015.

[13] S. Wang, D. Li, C. Sun, S. Yang, Y. Guan, and H. He, "Synthesis and characterization of g-C_3N_4/Ag_3VO_4 composites with significantly enhanced visible-light photocatalytic activity for triphenylmethane dye degradation," *Applied Catalysis B: Environmental*, vol. 144, pp. 885–892, 2014.

[14] X. Bai, L. Wang, R. Zong, and Y. Zhu, "Photocatalytic activity enhanced via g-C3N4Nanoplates to nanorods," *The Journal of Physical Chemistry C*, vol. 117, no. 19, pp. 9952–9961, 2013.

[15] Y. Zhang, M. Yan, S. Ge, C. Ma, J. Yu, and X. Song, "An enhanced photoelectrochemical platform: graphite-like carbon nitride nanosheet-functionalized ZnO nanotubes," *Journal of Materials Chemistry B*, vol. 4, no. 29, pp. 4980–4987, 2016.

[16] Y. S. Jun, E. Z. Lee, X. Wang, W. H. Hong, G. D. Stucky, and A. Thomas, "From melamine-cyanuric acid supramolecular aggregates to carbon nitride hollow spheres," *Advanced Functional Materials*, vol. 23, no. 29, pp. 3661–3667, 2013.

[17] D. Zheng, C. Pang, Y. Liu, and X. Wang, "Shell-engineering of hollow g-C_3N_4 nanospheres via copolymerization for photocatalytic hydrogen evolution," *Chemical Communications*, vol. 51, no. 47, pp. 9706–9709, 2015.

[18] Z. Zeng, K. Li, L. Yan et al., "Fabrication of carbon nitride nanotubes by a simple water-induced morphological transformation process and their efficient visible-light photocatalytic activity," *RSC Advances*, vol. 4, no. 103, pp. 59513–59518, 2014.

[19] S. H. Lai, Y. L. Chen, L. H. Chan, Y. M. Pan, X. W. Liu, and H. C. Shih, "The crystalline properties of carbon nitride nanotubes synthesized by electron cyclotron resonance plasma," *Thin Solid Films*, vol. 444, no. 1-2, pp. 38–43, 2003.

[20] Z. Huang, F. Li, B. Chen, and G. Yuan, "Porous and low-defected graphitic carbon nitride nanotubes for efficient hydrogen evolution under visible light irradiation," *RSC Advances*, vol. 5, no. 124, pp. 102700–102706, 2015.

[21] K. Li, Z. Zeng, L. Yan et al., "Fabrication of platinum-deposited carbon nitride nanotubes by a one-step solvothermal treatment strategy and their efficient visible-light photocatalytic activity," *Applied Catalysis B: Environmental*, vol. 165, pp. 428–437, 2015.

[22] J. W. Lee, H. J. Jeon, H.-J. Shin, and J. K. Kang, "Superparamagnetic Fe_3O_4 nanoparticles–carbon nitride nanotube hybrids for highly efficient peroxidase mimetic catalysts," *Chemical Communications*, vol. 48, no. 3, pp. 422–424, 2012.

[23] C. O. Song, W. H. Shin, H. S. Choi, and J. K. Kang, "Fabrication of size-controlled co nanoparticles via mediation of H-adatoms on pyridine-like nitrogen of carbon nitride nanotubes and their superior catalytic performance for hydrogen generation," *Journal of Materials Chemistry*, vol. 20, no. 34, p. 7276, 2010.

[24] H. Lee, S. M. Dellatore, W. M. Miller, and P. B. Messersmith, "Mussel-inspired surface chemistry for multifunctional coatings," *Science*, vol. 318, no. 5849, pp. 426–430, 2007.

[25] Z. Yu, F. Li, Q. Yang, H. Shi, Q. Chen, and M. Xu, "Nature-mimic method to fabricate polydopamine/graphitic carbon nitride for enhancing photocatalytic degradation performance," *ACS Sustainable Chemistry & Engineering*, vol. 5, no. 9, pp. 7840–7850, 2017.

[26] Y. Liu, H. Zhang, J. Ke et al., "0D (MoS_2)/2D (g-C_3N_4) heterojunctions in Z-scheme for enhanced photocatalytic and electrochemical hydrogen evolution," *Applied Catalysis B: Environmental*, vol. 228, pp. 64–74, 2018.

[27] Y. Yuan, R. T. Guo, L. F. Hong et al., "Recent advances and perspectives of MoS2-based materials for photocatalytic dyes degradation: a review," *Colloids and Surfaces A: Physicochemical and Engineering Aspects*, vol. 611, pp. 125836–125836, 2021.

[28] S. V. Vattikuti, C. Byon, and C. V. Reddy, "Synthesis of MoS_2 multi-wall nanotubes using wet chemical method with H_2O_2 as growth promoter," *Superlattices and Microstructures*, vol. 85, pp. 124–132, 2015.

[29] K. Ke, J. Liu, H. Sun et al., "Facile assembly of Bi_2O_3/Bi_2S_3/-MoS_2*n-p* heterojunction with layered *n*-Bi_2O_3 and *pS*-MoS_2 for enhanced photocatalytic water oxidation and pollutant degradation," *Applied Catalysis B: Environmental*, vol. 200, pp. 47–55, 2017.

[30] D. Wu and L. Han, "Solvothermal synthesis and characterization of visible-light-active MoO_3/MoS_2 heterostructure," *Journal of Sol-Gel Science and Technology*, vol. 91, no. 3, pp. 441–445, 2019.

[31] W. Jian, X. Cheng, Y. Huang et al., "Arrays of ZnO/MoS_2 nanocables and MoS_2 nanotubes with phase engineering for bifunctional photoelectrochemical and electrochemical water splitting," *Chemical Engineering Journal*, vol. 328, pp. 474–483, 2017.

[32] L. Ge, C. Han, X. Xiao, and L. Guo, "Synthesis and characterization of composite visible light active photocatalysts MoS_2-g-C_3N_4 with enhanced hydrogen evolution activity," *International Journal of Hydrogen Energy*, vol. 38, no. 17, pp. 6960–6969, 2013.

[33] J. Gao, Y. Zhou, Z. Li, S. Yan, N. Wang, and Z. Zou, "High-yield synthesis of millimetre-long, semiconducting carbon nitride nanotubes with intense photoluminescence emission and reproducible photoconductivity," *Nanoscale*, vol. 4, no. 12, pp. 3687–3692, 2012.

[34] S. Liu, F. Chen, S. Li, X. Peng, and Y. Xiong, "Enhanced photocatalytic conversion of greenhouse gas CO_2 into solar fuels over g-C_3N_4 nanotubes with decorated transparent ZIF-8 nanoclusters," *Applied Catalysis B: Environmental*, vol. 211, pp. 1–10, 2017.

[35] C. Song, S.-J. Park, and S. Kim, "Effect of modification by Polydopamine and polymeric carbon nitride on methanol oxidation ability of Pt catalysts-supported on reduced Graphene oxide," *Journal of the Electrochemical Society*, vol. 163, no. 7, pp. F668–F676, 2016.

[36] D. Gao, Q. Xu, J. Zhang et al., "Defect-related ferromagnetism in ultrathin metal-free g-C_3N_4 nanosheets," *Nanoscale*, vol. 6, no. 5, pp. 2577–2581, 2014.

[37] F. He, G. Chen, Y. Yu, Y. Zhou, Y. Zheng, and S. Hao, "The synthesis of condensed C-PDA-g-C_3N_4 composites with superior photocatalytic performance," *Chemical Communications*, vol. 51, no. 31, pp. 6824–6827, 2015.

[38] J. Kovger, A. Naujokaitis, G. Niaura, J. Juodkazyte, G. Valušis, and A. Jagminas, "Research on hydrothermal decoration of TiO2nanotube films with nanoplatelet MoS2species," *Nanomaterials and Nanotechnology*, vol. 6, p. 37, 2016.

[39] W. Li, G. Zhang, W. Sheng et al., "Engineering plasmonic Ag/AgCl-polydopamine-carbon nitride composites for enhanced photocatalytic activity based on mussel chemistry," *RSC Advances*, vol. 6, no. 108, pp. 106697–106704, 2016.

[40] J. Wang, J. Liu, H. Yang, Z. Chen, J. Lin, and Z. X. Shen, "Active sites-enriched hierarchical MoS2nanotubes: highly active and stable architecture for boosting hydrogen evolution and lithium storage," *Journal of Materials Chemistry A*, vol. 4, no. 20, pp. 7565–7572, 2016.

[41] Z. Wang, F. Tang, H. Fan, L. Wang, and Z. Jin, "Polydopamine generates hydroxyl free radicals under ultraviolet-light illumination," *Langmuir*, vol. 33, no. 23, pp. 5938–5946, 2017.

[42] H. K. Sadhanala, S. Senapati, K. V. Harika, K. K. Nanda, and A. Gedanken, "Green synthesis of MoS2nanoflowers for efficient degradation of methylene blue and crystal violet dyes under natural sun light conditions," *New Journal of Chemistry*, vol. 42, no. 17, pp. 14318–14324, 2018.

[43] S. Luo, S. Dong, C. Lu et al., "Rational and green synthesis of novel two-dimensional WS_2/MoS_2 heterojunction *via* direct exfoliation in ethanol-water targeting advanced visible-light-responsive photocatalytic performance," *Journal of HColloid and Interface Science*, vol. 513, no. 1, pp. 389–399, 2018.

[44] S. Kavitha, N. Jayamani, and D. Barathi, "Investigation on SnO_2/TiO_2 Nanocomposites and their Enhanced Photocatalytic Properties for the Degradation of Methylene Blue under

Solar Light Irradiation," *Bulletin of Materials Science*, vol. 44, no. 1, 2021.

[45] V. K. Nguyen, V. N. Nguyen Thi, H. H. Tran, T. P. Tran Thi, T. T. Truong, and V. Vo, "A facile synthesis of g-C3N4/BaTiO3 photocatalyst with enhanced activity for degradation of methylene blue under visible light," *Bulletin of Materials Science*, vol. 44, no. 1, 2021.

[46] S. Shenoy, K. Tarafder, and K. Sridharan, "Graphitic C3N4/CdS composite photocatalyst: synthesis, characterization and photodegradation of methylene blue under visible light," *Physica B: Condensed Matter*, vol. 595, no. 15, p. 412367, 2020.

[47] X. Zhao, X. Zhang, D. Han, and L. Niu, "Ag supported Z-scheme $WO_{2.9}$/g-C_3N_4 composite photocatalyst for photocatalytic degradation under visible light," *Applied Surface Science*, vol. 501, p. 144258, 2020.

[48] H. Chen, W. Cai, X. Gao, J. Luo, and X. Su, "PABA-assisted hydrothermal fabrication of $W_{18}O_{49}$ nanowire networks and its transition to WO_3 for photocatalytic degradation of methylene blue," *Advanced Powder Technology*, vol. 29, no. 5, pp. 1272–1279, 2018.